KfK 2689
Juni 1978

Thermodynamic Calculation and Experimental Determination of the Equation of State of Oxide Fuels up to 5000 K

M. Bober, W. Breitung, H. U. Karow
Institut für Neutronenphysik und Reaktortechnik
Projekt Schneller Brüter

Kernforschungszentrum Karlsruhe

KERNFORSCHUNGSZENTRUM KARLSRUHE

Institut für Neutronenphysik und Reaktortechnik
Projekt Schneller Brüter

KfK 2689

Thermodynamic Calculation and Experimental Determination of the Equation of State of Oxide Fuels up to 5000 K

M.Bober, W.Breitung, H.U.Karow

presented at the IAEA Specialists' Meeting on Equations of State of Materials of Relevance to the Analysis of Hypothetical Fast Breeder Reactor Accidents, Harwell, UK, June 19-23, 1978.

Kernforschungszentrum Karlsruhe GmbH., Karlsruhe

Abstract

The safety analysis of fast reactors requires the knowledge of the thermodynamic data of state of the nuclear fuel materials up to 5000 K. Based on the law of mass action, the saturation vapor pressure curves p(T) have been calculated for uranium dioxide and stoichiometric and hypostoichiometric (U,Pu) mixed oxide up to 5000 K. The functions used of the free energies of formation and of the oxygen potentials and the resulting partial vapor pressures are represented. The present scatter of the input data leads to a tolerable uncertainty of the calculated equations of state of $\Delta p/p \approx \pm 50\%$.

Vapor pressure measurements at very high temperatures require the application of dynamic measuring methods with pulse heating. The potential is discussed of the various experimental techniques: electrical resistive heating, electron beam heating, neutron pulse heating, and laser beam heating. A measuring method using a laser heating technique is described. Vapor pressure measurements with liquid UO_2 up to 4200 K are reported. The resulting vapor pressure data fairly well agree with the calculated equation of state of $UO_{2.00}$. - For pyrometric measurements of liquid fuel the exact value of the spectral emissivity of the fuel surface is needed which depends on temperature. Measurements of the emissivity of liquid UO_2 at 0.65 µm are shortly described.

Thermodynamische Berechnung und experimentelle Bestimmung der Zustandsgleichung von Oxidbrennstoffen bis 5000 K

Zusammenfassung

Die Sicherheitsanalyse schneller Reaktoren erfordert die Kenntnis der thermodynamischen Zustandsdaten des Brennstoffs bis 5000 K. Mit Hilfe des Massenwirkungsgesetzes wurden die Sättigungsdampfdruckkurven p(T) von Urandioxid und von stöchiometrischem und unterstöchiometrischem (U,Pu)-Mischoxid bis 5000 K berechnet. Die verwendeten Beziehungen für die freien Bildungsenthalpien und die Sauerstoffpotentiale sowie die resultierenden Partialdampfdrucke werden wiedergegeben. Aus der gegenwärtigen Fehlerbreite der Eingabedaten resultiert eine tolerierbare Unsicherheit der errechneten Dampfdruckkurven der Oxidbrennstoffe von $\Delta p/p \approx \pm 50\%$.

Dampfdruckmessungen bei sehr hohen Temperaturen erfordern die Anwendung dynamischer Meßmethoden mit Pulsheiztechniken. Das Potential der folgenden experimentellen Techniken wird diskutiert: Elektrische Widerstandsheizung, Elektronenstrahlheizung, Neutronenpulsheizung und Laserstrahlheizung. Eine Meßmethode, die eine Laserheiztechnik verwendet, wird beschrieben und die Ergebnisse der Dampfdruckmessungen an flüssigem UO_2 bis 4200 K werden wiedergegeben. Die Ergebnisse stimmen gut mit der berechneten Zustandsgleichung von $UO_{2.00}$ überein. - Die pyrometrische Temperaturbestimmung von flüssigem Brennstoff setzt die Kenntnis des spektralen Emissionsvermögens der Brennstoffoberfläche voraus. Messungen des Emissionsvermögens von flüssigem UO_2 bei 0.65µm werden kurz beschrieben.

CONTENTS

1. INTRODUCTION

Equation of State (EOS) data of reactor core materials are required up to temperatures of about 5000 K for analysing Hypothetical Core Disruptive Accidents (HCDA). These are the vapor pressures, liquid specific heats, liquid densities, and the enthalpies of phase change. In addition the high temperature values of compressibility, expansivity, viscosity, surface tension, thermal conductivity and emissivity are of interest. The EOS data of the fuel and those of the gaseous and volatile fission products are important in the first place. In recent time some knowledge has been gained on EOS data of liquid oxide fuel /1/, which are important first of all for the accident analysis of reactors operated with fresh fuel.

In transient thermomechanical calculations of the HCDA analysis the total vapor pressure as a function of enthalpy must be known. However, most of information about the vapor pressure is available in the pressure versus temperature format. This means that its application in such an analysis calls for the extreme temperature heat capacity to be measured or estimated in addition. The knowledge of the actual temperature development in an HCDA, on the other hand, is necessary to calculate heat transport processes and to estimate the reaction kinetics of the chemical processes involved. Furthermore, it is advantageous for calculating the effect of the Doppler coefficient which is normally given as a function of temperature.

Primary information about fuel vapor originates in high temperature static measurements performed up to or slightly above the melting point. In this temperature range, the energies of formation and phase change and the oxygen potential have been measured rather precisely. These measurements yielded a relatively great number of reliable data which were critically selected and compiled /2-4/. Based on an extrapolation of these data, the law of mass action allows to calculate the saturation vapor pressure of oxide fuel up to about 5000 K /3/. Underlying the present scatter of the input data in the variance analysis leads to a tolerable uncertainty margin of the resulting vapor pressure curve. Nevertheless, such calculation alone cannot be completely satisfactory. In the very high temperature region the physical structure of the liquid and the physical phenomena of intensive evaporation should be taken into account. For example, physical processes such as ionization and excitation may become important /5/. Therefore, direct vapor pressure measurements are indispensible to confirm the calculated vapor pressures.

Vapor pressure measurements at such extreme temperatures can only be accomplished with dynamic pulse heating methods because suitable crucible materials are lacking. All these dynamic methods are more or less complicated and demand great efforts for sufficiently accurate determination of the measuring quantities. The measurement of the vapor pressure versus temperature requires the exact determination of the evaporation temperature, which is difficult and becomes very problematic above

some 4500 K. The evaluation of the vapor pressure as a function of energy calls for the exact determination of the internal energy of the condensed phase which is likewise difficult. Besides, it is a problem to get results from the experiments that really correspond to the condition of saturated liquid vapor equilibrium.

2. VAPOR PRESSURE CALCULATION OF OXIDE FUEL UP TO 5000 K BASED ON THE LAW OF MASS ACTION

To get a reliable data basis of oxide fuel vapor pressures for the HCDA analysis the direct measurements at the very high temperatures should be accompanied by calculations of the vapor pressure curve. The following theoretical approaches exist for the determination of the EOS of oxide fuels up to very high temperatures:

a) the theory of corresponding states,
b) the method of rectilinear diameters,
c) the theory of significant liquid structures, and
d) the law-of-mass-action calculation method.

The last method - based on the law of mass action - has the advantage that it is a transparent method, physically approved, for which a relatively broad basis already exists of the data required. Therefore, this method seems to be the most appropriate one for calculating oxide fuel vapor pressures up to temperatures of 5000 K /6,3/, which are of main interest for the HCDA analysis.

It is well known that the equilibrium vapor pressure of gaseous species $MO_B(g)$ evaporating from a solid or liquid metal oxide $MO_A(cond.)$ can be calculated from the evaporation reaction:

$$MO_A(cond.) + \frac{B-A}{2} O_2(g) \rightarrow MO_B(g) \qquad (2.1)$$

This reaction includes also the evaporation of pure metals (A=B=0). For thermodynamic equilibrium the law of mass action gives

$$\Delta G^{o}_{f,T}\left[MO_B\right] - \Delta G^{o}_{f,T}\left[MO_A\right] + RT \ln \frac{p_{MO_B}}{a_{MO_a} \cdot p_{O_2}^{(B-A)/2}} = 0 \qquad (2.2)$$

or with $RT \ln p_{O_2} = \Delta\bar{G}_{O_2}$

$$\text{Log } P_{MO_B} = \log a_{MO_A} + \frac{\Delta G^{o}_{f,T}\left[MO_A\right] - \Delta G^{o}_{f,T}\left[MO_B\right] + \frac{B-A}{2}\Delta\bar{G}_{O_2}}{RT \ln 10} \qquad (2.3)$$

where the variables have the following meanings:

P_{MO_B} = vapor pressure of the gaseous metal oxide, MO_B.

a_{MO_A} = activity of the metal oxide in the condensed phase, MO_A.

$\Delta G^{\circ}_{f,T}\left[MO_A\right]$ = free enthalpy of formation of the condensed oxide, MO_A, at temperature, T.

$\Delta G^{\circ}_{f,T}\left[MO_B\right]$ = free enthalpy of formation of the gaseous oxide, MO_B, at temperature, T.

$\Delta\bar{G}_{O_2}$ = oxygen potential of the oxide system.

If the thermodynamic variables on the right side of Eq. (2.3) are known, the vapor pressure of each of the gaseous species MO_B can be calculated.

2.1. Vapor pressure of Liquid UO_2

The dominant vapor species above liquid UO_2 are, in decreasing order, $UO_2(g)$, $UO_3(g)$, $O(g)$ and $O_2(g)$. If we introduce the following abbreviations for the oxygen potential and the standard free energies of formation

$x_1 = \Delta\bar{G}_{O_2}$, and

$x_2 = \Delta G^{\circ}_{f,T}\left[\bar{U}O_2(\ell)\right]$ for liquid UO_2,

$x_3 = \Delta G^{\circ}_{f,T}\left[\bar{U}O_2(g)\right]$ for gaseous UO_2,

$x_4 = \Delta G^{\circ}_{f,T}\left[\bar{U}O_3(g)\right]$ for gaseous UO_3 and

$x_5 = \Delta G^{\circ}_{f,T}\left[\bar{O}(g)\right]$ for oxygen gas,

the total vapor pressure of liquid UO_2 can be approxinated by

$$p = P_{UO_2} + P_{UO_3} + P_{oxygen}$$

$$= \exp\left(\frac{x_2-x_3}{RT}\right) + \exp\left(\frac{x_2-x_4+x_1/2}{RT}\right) + \gamma\cdot\exp\left(\frac{x_1}{RT}\right) . \qquad (2.4)$$

$$P_{oxygen} = P_O+P_{O_2} \ , \ P_O = P_{O_2}^{1/2}\exp(-x^5/RT), \ \gamma=(2P_O+P_{O_2})/P_{oxygen}.$$

R and T are the gas constant and temperature, respectively.

Each of the thermodynamic variables x_i is subject to certain error limits. If $\sigma^2_{x_i}$ is the variance of the variable x_i the variance of the total vapor pressure σ^2_p is given by /7/

$$\sigma_p^2 = \sum_{i=1}^{5} \left(\frac{\partial p}{\partial x_i}\right)^2 \sigma^2_{x_i} \qquad (2.5)$$

The highest weight belongs to the variance of the free energy of formation of liquid UO_2, followed by that of gaseous UO_2 and of gaseous UO_3 which equally contribute to σ_p^2. The weigths of $\sigma^2_{x_3}$ and $\sigma^2_{x_4}$ are <30% of the weight of $\sigma^2_{x_2}$. The variances of the oxygen potential and of the gaseous oxygen free energy of formation have even less weight up to temperatures of 4500 K.

To estimate the actual uncertainties in the thermodynamic variables x_i, the data available were plotted as a function of temperature up to 5000 K. Figs.2.1a and 2.1b show the published free energies of formation of solid and liquid UO_2, respectively /4,6,8-13/. The uncertainty, being less than 10 kJ/mol in the solid region, should be expected to increase in the liquid region. In Fig. 2.2, the available free energies of gaseous UO_2 are plotted up to 5000 K /4,8,10, 11,14,15/. The uncertainty should be $\leq$ 40 kJ/mol at 5000 K.

The dashed lines shown in Figs.2.1b and 2.2 represent the values which are chosen as the most probable ones. These values have been used in the vapor pressure calculations. The bars at 3300 K, 4000 K, and 5000 K show the standard deviations σ_{x_i} as estimated from the error margins of the various data. At 5000 K, for instance, σ_{x_2} and σ_{x_3} are taken to be 20 kJ/mol. From similar diagrams (x_1:/16,17/; x_4:/11,18-21/; x_5:/22/) the remaining standard deviations were estimated to be at 5000 K: σ_{x_1}=45 kJ/mol, σ_{x_4}=20 kJ/mol, and σ_{x_5}=15 kJ/mol. If we assume a Gaussian probability distri-

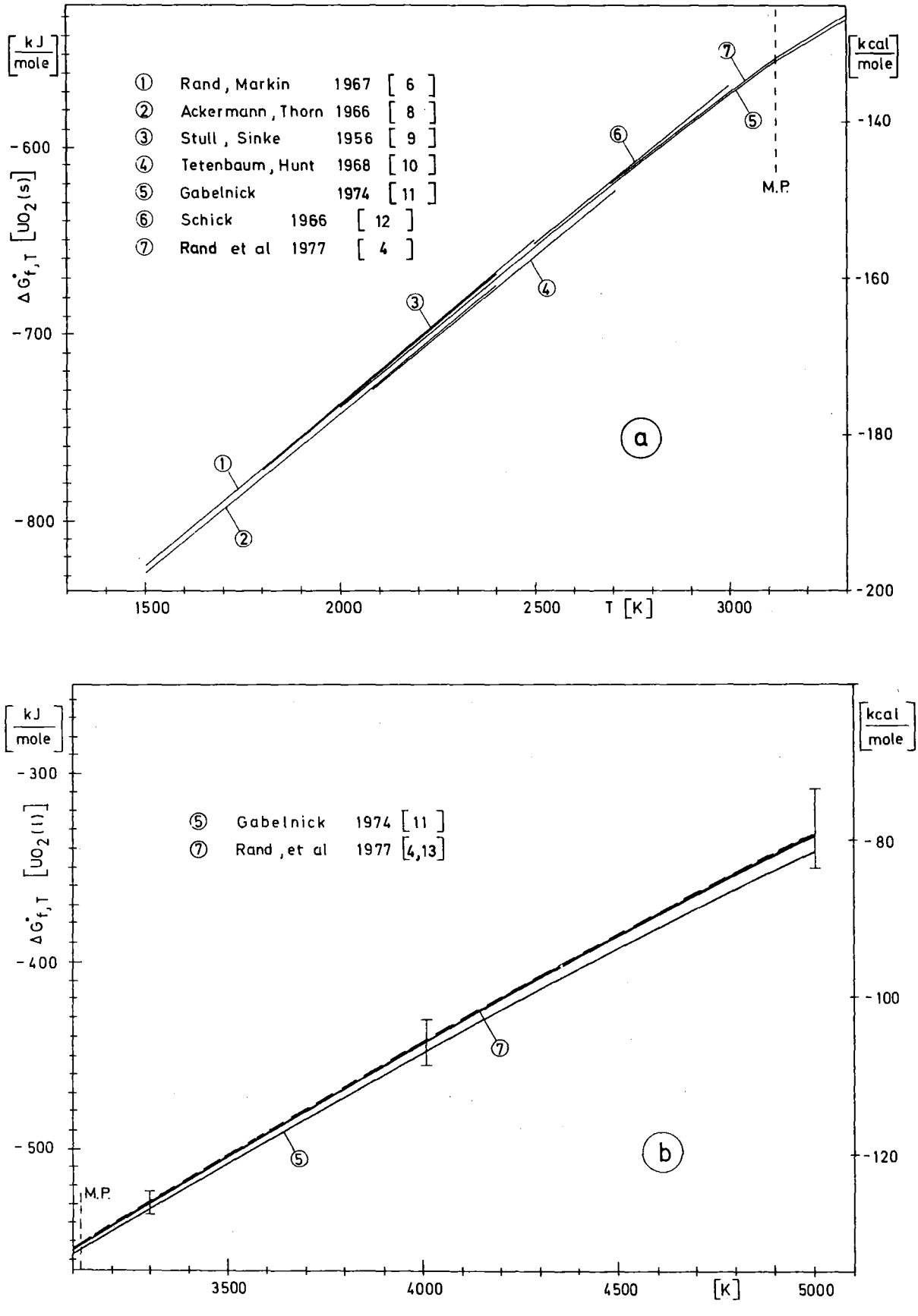

Fig. 2.1 Free energies of formation of solid and liquid UO_2 as a function of temperature.

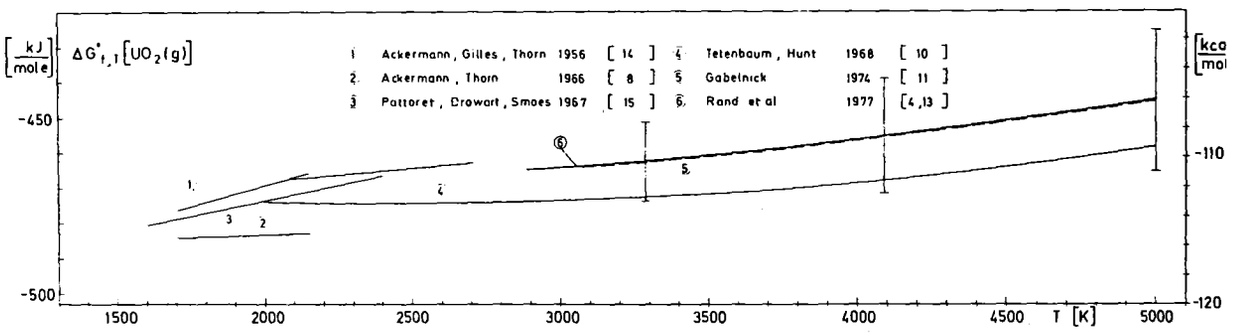

Fig. 2.2 Free energies of formation of gaseous UO_2 as a function of temperature.

bution around the most probable value μ_i of the variable x_i:

$$Pr(x_i) = \frac{1}{\sigma_{x_i}\sqrt{2\pi}} \exp\left(-\frac{1}{2}(x_i-\mu_i)^2/\sigma_{x_i}^2\right) \qquad (2.6)$$

the probability to find the true value of the quantity x_i within the one-σ-band (Fig. (2.3), is about 70%.

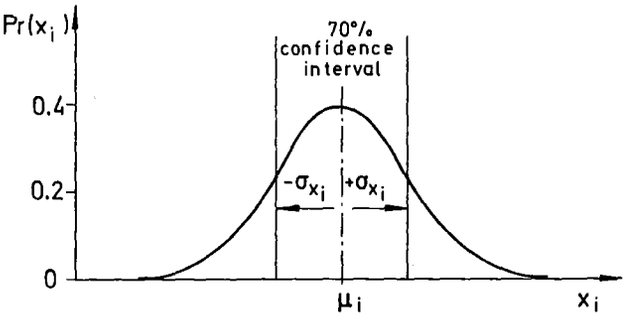

Fig. 2.3 Gaussian probability distribution around the most probable value μ_i of the quantity x_i.

Introducing the most probable values of the quantities x_i in Eq.(2.4), and the above standard deviations σ_{x_i} in Eq.(2.5) yields the most probable vapor pressure curve p(T) with the total standard deviation $\sigma_p(T)$ shown in Fig.2.4. The dashed lines indicate the confidence limits such that the true total vapor pressure of UO_2 can be expected to lie within this band with a probability of about 70%.

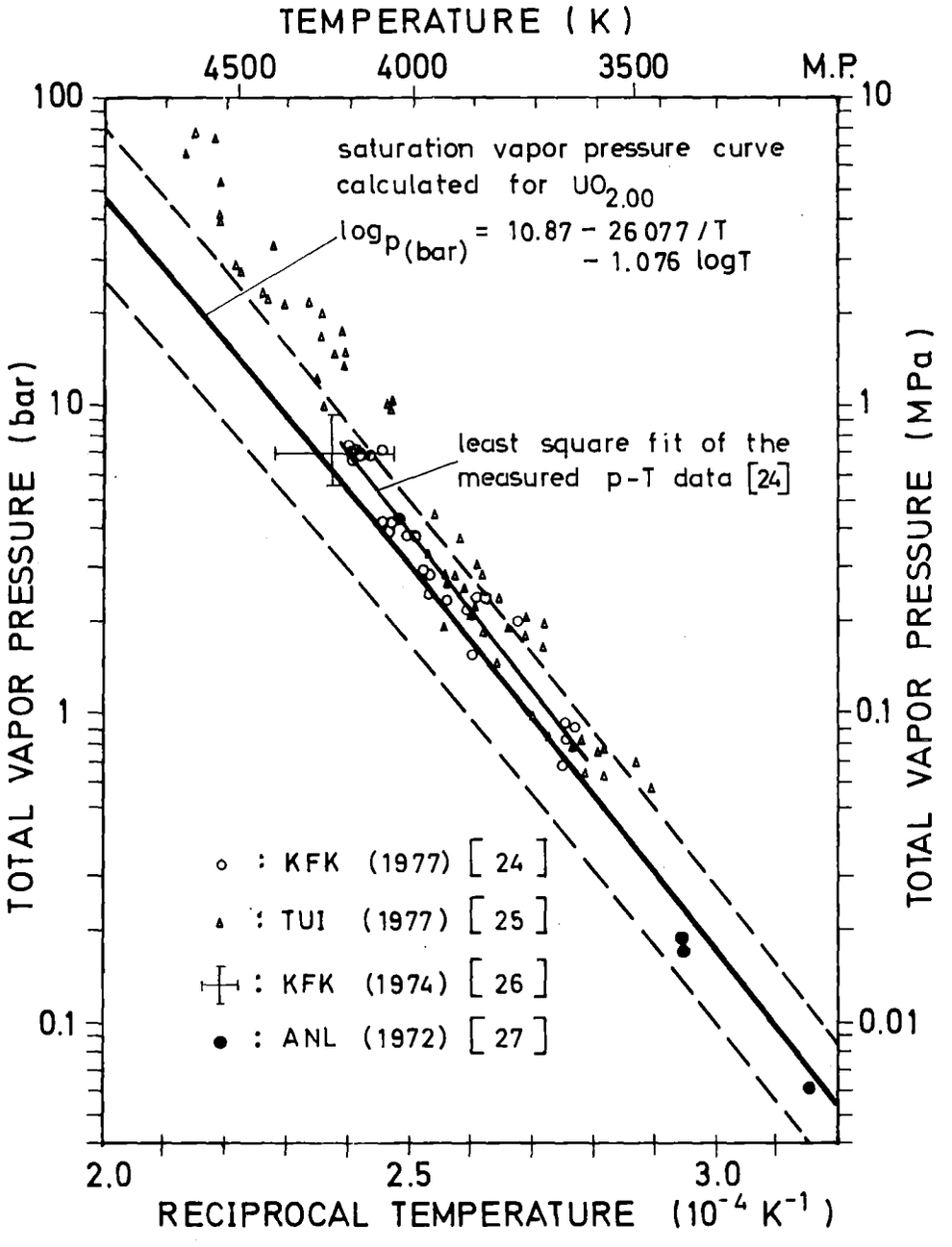

Fig.2.4 Most probable, calculated vapor pressure curve for the liquid-vapor equilibrium (EOS) of $UO_{2.00}$ (bulk line). The dashed lines denote the confidence interval for 70%. The symbols represent experimental vapor pressure values obtained in measurements with laser evaporation /24-26/ (open evaporation) and with transpiration techniques /27/.

The calculated total vapor pressure curve of liquid UO_2 up to 5000 K can be represented by the equation:

$$\log p = 10.87 - 26077/T - 1.076 \log T \quad \text{(bar)}. \qquad (2.7)$$

Formal application of the Clausius-Clapeyron equation leads to the apparent heat of evaporation

$$\Delta H = 499 - 0.009\ T \quad \text{(kJ/mol)}. \qquad (2.8)$$

The uncertainty in the calculated total vapor pressure, $\Delta p/p \approx \pm 50\%$, is most effectively reduced by reducing the error limits of the free energies of formation of liquid UO_2 and of gaseous UO_2 and UO_3. Therefore future work relating to the UO_2 vapor pressure calculation should deal with the more precise determination of the heat capacity of $UO_2(\ell)$ and of the free energies of formation of $UO_2(g)$ and $UO_3(g)$.

For comparison also the vapor pressure data of UO_2 evaluated from laser evaporation /24-26/ and transpiration measurements /27/ are given in Fig. 2.4. These experimental vapor pressures partly agree with the calculations. Apart from the measurements at temperatures above 4200 K, which still need to be converted to closed system conditions, the measurements show fairly good agreement with the calculated curve within the given confidence limits. The vapor pressure curve of liquid $UO_{2.00}$ recently recommended by the IWGFR*) /46/ comes close to the experimental curve /24/.

---

*) The $UO_{2.00}$ vapor pressure curve recommended by the IWGFR/IAEA is given by $\log (p_{total}/\text{bar}) = 29.65 - 34930/T - 5.64 \log T$.

The present experimental uncertainties do not allow to deduce the slope of the vapor pressure curve so as to allow a rather likely extrapolation to temperatures above 5000 K. Future measurements should be aimed at diminishing the experimental scatter and minimizing possible systematic errors.

The following equations for the mean oxygen potential and free energy functions were used in the above calculations:

$$\Delta\bar{G}_{O_2}(UO_2) = -3423+0.092\ T + 823.8\ \log T \quad \text{kJ/mol}, \quad (2.9)$$

$$\Delta G_f[\underline{U}O_2(\ell)] = -2088+0.0773\ T + 370.6\ \log T \quad \text{kJ/mol}, \quad (2.10)$$

$$\Delta G_f[\underline{U}O_2(g)] = -124.9+0.02186\ T - 116.2\ \log T \quad \text{kJ/mol}, \quad (2.11)$$

$$\Delta G_f[\underline{U}O_3(g)] = -873.8+0.09356\ T \quad \text{kJ/mol}, \quad (2.12)$$

$$\Delta G_f[\underline{O}(g)] = 257.4-0.0676\ T \quad \text{kJ/mol}. \quad (2.13)$$

These functions represented by Eqs.(2.9) to (2.13), together with the standard deviations given in Sec. 2.1, cover the scatter in the values of the various data sources, cited in Sec.2.1. The validity of the equations ranges from the melting point of UO_2 to 5000 K. In the diagrams for UO_2, shown in Figs.2.1 and 2.2, the dashed lines represent the functions (2.10) and (2.11).

2.2 Vapor Pressure of Liquid (U,Pu) Mixed Oxide

The vapor pressures of (U,Pu) mixed oxides can be calculated with the law of mass action, assuming an ideal solution of uranium- and plutonium oxide. There are several theoretical and experimental results supporting this assumption:

a) The melting and solidification temperatures of $(U_{1-y}Pu_y)O_2$ follow the ideal solution laws /23/.

b) The lattice parameters of $(U_{1-y}Pu_y)O_2$ are a linear function of the plutonium content y (Vegard's Law) /23/.

c) The comparison of the free energies of UO_2, PuO_{2-z}, and $(U_{1-y}Pu_y)O_{2-x}$ at 1150 K indicates ideal solution of UO_2 and PuO_{2-z} /6/.

d) Vapor pressures of solid (U,Pu) mixed oxides, calculated on the assumption of ideal solution, show good agreement with existing vapor pressure measurements /3 (Figs. 8+9)/.

In the following paragraphs the vapor pressure of hypostoichiometric (U,Pu) mixed oxide will be considered especially because this fuel is of interest in the initial phase of reactor operation. For the vapor pressure calculations it was assumed that one mole of $(U_{0.80}Pu_{0.20})O_{2-x}$ is an ideal solution of 0.80 mole uranium oxide and 0.20 mole plutonium oxide. The dominant vapor species above this mixed oxide are - as in the case of pure uranium oxide - $UO_2(g)$, $UO_3(g)$, $O(g)$ and $O_2(g)$. Therefore the total vapor pressure above $(U_{0.80}Pu_{0.20})O_{2-x}$ can be approximated, similar to Eq.2.4, by

$$P_{total} = 0.8 \exp\left(\frac{x_2-x_3}{RT}\right) + 0.8 \exp\left(\frac{x_2-x_4+x_1/2}{RT}\right) + \gamma \exp\left(\frac{x_1}{RT}\right) \qquad 2.14)$$

For the thermodynamic variables x_2 to x_5, the same values have been used, as in the case of UO_2. Values for x_1, the oxygen potential of the (U,Pu) mixed oxide, were calculated from two existing oxygen potential models /16,17/. At 5000 K the results differ for about 100 kJ/mol. The mean of these two values and σ_{x_1}=50 kJ/mol was used to calculate P_{total} and its variance.

The resulting saturation vapor pressure curves are shown in Fig.2.5 for three stoichiometric states of the mixed oxide. In the temperature region up to 4500 K an uncertainty margin of $\Delta p/p \approx \pm 50\%$ is obtained for each curve which belongs to a confidence interval of 70%. The most probable vapor pressure curves up to 5000 K can be described by the equations

$$\log p_{total} = 10.75 - 26276/T - 1.006 \log T \quad \text{(bar)} \qquad (2.15)$$

for $(U_{0.8}Pu_{0.2})O_{1.95}$,

$$\log p_{total} = 7.49 - 23830/T - 0.2465 \log T \quad \text{(bar)} \qquad (2.16)$$

for $(U_{0.8}Pu_{0.2})O_{1.97}$, and

$$\log p_{total} = -5.73 - 16070/T + 2.928 \log T \quad \text{(bar)} \qquad (2.17)$$

for $(U_{0.8}Pu_{0.2})_{2.00}$.

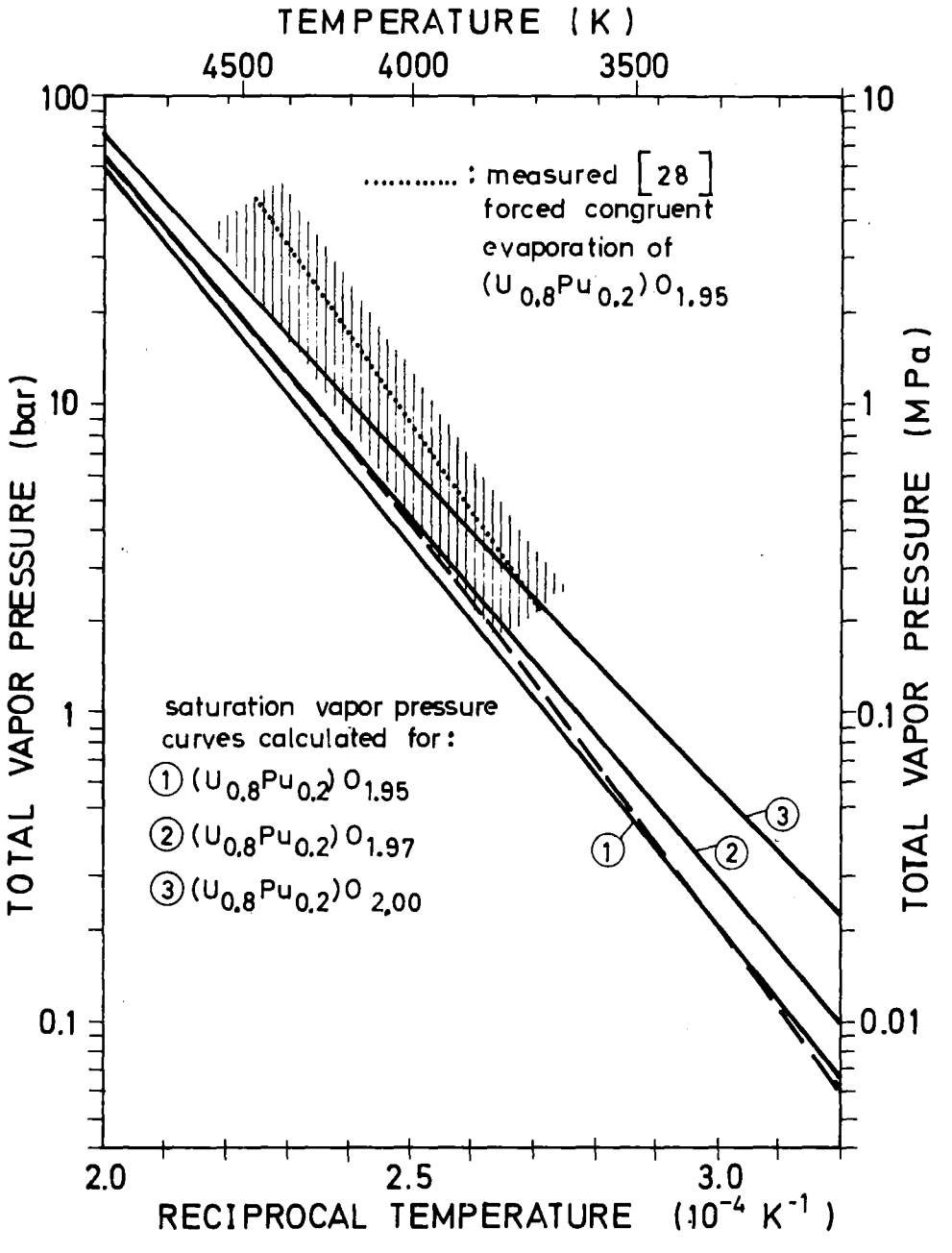

Fig. 2.5 Most probable, calculated vapor pressure curves for the liquid vapor equilibrium (EOS) of $(U_{0.8}Pu_{0.2})O_{2-x}$, (solid lines). The dotted line represents the vapor pressure curve obtained by Ohse et al. /28/ from open congruent evaporation experiments. This curve still needs to be converted to closed system conditions. The shadowed area indicates the minimum experimental error margin. For comparison the dashed line gives the equation of state of $UO_{2.00}$ recommended by the IWGFR/IAEA /46/ (s.footnote p.10).

Formal application of the Clausius-Clapeyron equation yields the apparent heats of evaporation

$$\Delta H(T)_{evap} = 503 - 0.0084\ T \qquad (kJ/mol) \qquad (2.18)$$

for $(U_{0.8}Pu_{0.2})O_{1.95}$,

$$\Delta H(T)_{evap} = 456 - 0.002\ T \qquad (kJ/mol) \qquad (2.19)$$

for $(U_{0.8}Pu_{0.2})O_{1.97}$, and

$$\Delta H(T)_{evap} = 308 + 0.024\ T \qquad (kJ/mol) \qquad (2.20)$$

for $(U_{0.8}Pu_{0.2})O_{2.00}$.

It can be seen from Fig.2.5 that the vapor pressure of hypostoichiometric mixed oxide $(U_{0.8}Pu_{0.2})O_{1.95...1.97}$ depends little on its actual stoichiometric state in the very high temperature range. Fig. 2.5 also contains the vapor pressure curve obtained by Ohse /28/ from open forced congruent evaporation experiments with $(U_{0.8}Pu_{0.2})O_{1.95}$. The thermodyanmic conversion to saturation vapor pressures (closed system conditions) would somewhat rise this experimental curve so that the agreement with the calculated curves diminishes (Chapter 3.4, page 22).

As shown by Fig.2.4 and Fig.2.5, the vapor pressure curve of liquid UO_2 fuel lies below the vapor pressure curves of mixed oxide fuels. So, because of the still existing theoretical and experimental uncertainties of the data of state of liquid mixed oxide fuels, it has been considered reasonable to use the UO_2 vapor pressure curve as the (pessimistic) equation of state of the oxide fuel in HCDA analysis, in order to be on the safe side in the calculation of the nuclear energy release /46/.

3. EXPERIMENTAL TECHNIQUES OF VAPOR PRESSURE MEASUREMENTS AT EXTREME TEMPERATURES

Vapor pressure measurements at the high temperatures above 3000 K require the application of dynamic pulse heating techniques. At the experimenters' disposal are the techniques of electrical resistive, electron beam, neutron pulse, and laser beam heating.

3.1. Electrical resistive heating

The technique of electrical resistive heating over subsecond times is chiefly suitable to study high-temperature thermophysical properties of metals /29/. Recently, at several laboratories fast pulse heating on a µs time scale was acieved by resistive heating of a wire or rod-shaped sample. The sample was enclosed either in an isobaric high-pressure gas atmosphere, being adjustable between 0 and 6 kilobars /30-32/, or it was embedded in a fluid environment /33/.

During the rapid impulse process - in the short interval before the sample changes into the liquid-vapor two-phase state - it is possible to investigate the metal in the solid and liquid states over a broad temperature range. From the measured current and voltage the electrical resistivity and the change in enthalpy of the sample can be computed up to near the critical point. Detection of the break in electrical conductivity at different environmental pressures allows to correlate the vapor pressure of the sample to its enthalpy. By fast photography and fast pyrometry its high-temperature thermal expansion and heat capacity can be estimated in addition /31/.

At all times during the pulse heating process the sample remains at least close to thermodynamic equilibrium. This is an advantage of the resistive heating technique. Problems may arise, e.g., from a non-uniform current distribution, which leads to inhomogeneous energy deposition and temperature distribution, or from a possible instability of the hot liquid-metal column.

In this connection the potential of direct electrical heating experiments with irradiated oxide fuel should be mentioned which helps to simulate effects of reactor transients, e.g., fuel expansion and fission gas behavior /34/.

3.2. Electron Beam Heating

Similar to the exploding wire technique high-energetic electron beam heating, also in a μs time scale, gives vapor pressure data as a function of enthalpy /35, 36/. This technique is applicable to ceramic fuel materials. Experiments with $U_{2.08}$ were performed with the Sandia Relativistic Electron Beam Accelerator (REBA) at energy levels up to 3000 J/g and vapor pressures up to about 1500 bars /36/.

The large penetration depth of the relativistic electron beam allows real volume heating of the evaporation sample in a closed system. The sample is confined within a cylindric crucible tightly closed by two thin pistons made of graphite which is a less electron absorbing material than the sample material. By measuring the piston expansion after electron pulse incidence, the total vapor pressure of the sample can be evaluated versus the electron energy deposited from mechanical equations of motion /35, 36/.

The technique of electron beam heating is appropriate for dense vapor studies in the region of very high temperatures above 5000 K. It is a promising method to determine the vapor pressures of oxide fuel over a high pressure and energy range up to the vicinity of the critical region.

Although absorption of high-energetic electrons is nearly uniform on the basis of energy per mass, complete equilibrium may be somewhat uncertain to attain during the rapid heating process. So, the heat capacity of the sample might be lower than in equilibrium state dependent on the heating rate /37,38/. This effect could produce uncertainties in the resulting vapor pressure curve. Another error source lies in the determination of the total energy absorbed in the sample. For UO_2 an uncertainty of ±5% in the energy deposit yields an uncertainty of some ±50% in the vapor pressure evaluation.

In order to relate the enthalpy to the temperature scale, knowledge is needed of the heat capacity of liquid oxide fuel. Vice versa, the consistency of the existing heat capacity models could in principle be proved by comparing vapor pressure data measured as a function of temperature with those measured as a function of enthalpy. A quantitative comparison, however, would require that the uncertainties in the determination of the p(H) data and of the p(T) data can be diminished.

3.3. Neutron Pulse Heating

Recently a technique was developed to get experimental vapor pressure data for reactor fuel materials from pulse fission heating /39/. First experiments were carried out with $UO_{2.08}$ in the Sandia Annular Core Pulse Reactor (ACPR) at energy levels up to 3000 J/g.

In these experiments fuel samples are enclosed in a graphite crucible within a pressure cell and exposed to fission heating over millisecond times. The pressure growth in the cell is monitored with a pressure transducer and the resulting fuel vapor pressure is evaluated as a function of fission energy.

Precise evaluated of the energy content of the heated sample is difficult due to nonuniformities in the distribution of fission energy deposited within the sample and the thermal losses from the sample. However, it is possible to estimate bounds on the energy content which limit its uncertainty margin to about ±10%. The corresponding uncertainty margin of the fuel vapor pressure curve is some ±70%.

An advantage of these in-pile experiments is the fact that the attainable heating rates are comparable to those anticipated during a fast reactor transient in a hypothetical accident. The measurements can be extended to mixed oxides, carbides, and to fuel with simulated fission product additives. Eventually, experiments with irradiated fuel samples are possible.

3.4. Laser Beam Heating

Laser pulse heating techniques were developed at Karlsruhe in order to determine the vapor pressure of ceramic fuel materials as a function of tempersture /26,40/. These techniques allow measurements up to 5000 K already at a reasonably limited expenditure of equipment. The length of the applicable laser heating pulses ranges from microseconds to milliseconds at power densities between some 10 and 1000 kW/cm^2. The application of long heating pulses with relative low power densities allows to extend the measurements down to temperatures of about 3500 K, i.e. below the boiling point of UO_2

where the results are directly adjoining that from conventional measurements /41/.

Owing to the high absorptivity of the target material for the laser light, the heated volume is restricted to a thin surface layer characterized by steep temperature gradients below the surface /42/. The vapor pressure has to be evaluated from the experimentally determined evaporation velocity existing under the condition of open surface evaporation. However, at high evaporation rates open surface evaporation implies a gasdynamic vapor flow which is quite different from a free molecular evaporation flow /26/. It requires a suitable evaluation model. The evaporation velocity can be determined either from measuring the reaction pressure of the vapor and the evaporated mass or from observing the evaporation crater depth. To achieve the temperature resolution of the evaporation velocity, the local temperature profile in the crater has to be measured.

The determination of the evaporation temperature must be handled with great care because of the exponential p(T) relationship. In a first approach an average evaporation temperature can be determined from the momentum of the vapor jet observed after its adiabatic expansion. However, based on the measured spectral emissivity of liquid oxide fuel /43/, the most practicable way of temperature measurement is by direct optical pyrometry. It allows spatial resolution of the surface temperature. The upper temperature limit of reliable pyrometric measurement with oxide fuel has been estimated to be about 4500 K. This application limit is derived from two effects, both enhanced with rising temperature. One is the existence of steep temperature gradients immediately below the evaporating surface, which diminishes the thermal emission of radiation, the other is the absorption of thermal radiation in the ionized vapor plume above the evaporating surface. - By analogy, an application limit of the vapor pressure

measurements is given by the onset of radiational interaction of the vapor plasma with the incident laser beam at temperatures of about 4500 K.

An enthalpy balance of the evaporation process is only feasible at temperatures above some 4000 K where open evaporation is so intensive that the absorbed laser energy mostly corresponds to the heat consumed in evaporation. The liquid surface layer remains thin and liquid movement in the crater is negligible. The measurement of the absorbed laser energy then allows to estimate the specific heat of the liquid fuel and its vapor pressure as a function of enthalpy. At lower temperatures the liquid surface layer becomes thicker and liquid material is caused to displace radially in the crater due to the reaction pressure of the vapor jet. This effect disturbs the enthalpy belance of the evaporation and also hinders the evaluation of the true crater depth caused by evaporation only.

Vapor pressure measurements in which the measuring variables are the evaporated mass and the reaction pressure of the vapor remain unaffected by a liquid movement.This allows to apply longer heating pulses in the ms range, which ensure steady-state conditions during evaporation. Longer pulses result in a higher accuracy of the measurements because they better average the evaporation rate. They equalize possible temperature oscillations or instabilities which might be caused by a liquid movement in the surface layer.

An important aspect arises from the condition of forced congruent evaporation, which underlies open surface evaporation of oxide fuel at the high evaporation rates under consideration /42,44/. In open evaporation, changes in composition occur in the evaporating surface of a multicomponent system. This is due to the depletion of the preferentially evaporating components in the evapo-

rating surface layer, which cannot be restored by diffusion from the bulk material. In the laser evaporation of oxide fuel, after a very short transient evaporation period (which is shorter than the laser pulse) the surface composition becomes stationary such that the integral vapor composition corresponds to the bulk composition of the fuel. In this forced congruent evaporation mode the composition of the evaporating surface layer differs considerably from the given fuel composition and depends on the actual evaporation temperature. Consequently, the total vapor pressures developing in open surface evaporation may depart appreciably from its thermodynamic EOS depending on the actual fuel material.

It can be concluded from thermodynamic calculations based on the law of mass action that the vapor pressure curve of UO_2 measured in open evaporation should deviate only insignificantly from the EOS up to temperatures of about 4500 K. However, measurements with liquid (U,Pu) mixed oxides, even if performed with strongly hypostoichiometric mixed oxides, could yield pressures of about half the corresponding EOS pressures or less /42/.

The evaluation of the heat of evaporation of the bulk material from the slope of the log p versus 1/T curve is not reliable because every evaporation temperature is related to another actual surface composition of the specimen. The required EOS, however, can be deduced from the measured vapor pressure curve by correcting all measured pressures in proportion to the calculated changes of composition in the evaporation surface /3, 45/. This correction is not strongly affected by the uncertainties of the underlying thermodynamic data because the calculated differences between the pres-

sures of the forced congruent evaporation curve and the EOS are actually based on the same set of data. Nevertheless, because of the remaining uncertainties in the evaluation model and due to experimental errors, the experimentally determined vapor pressures corrected to EOS pressures should be viewed as realistic only within an uncertainty of at least ±50%.

3.5. Conclusions

The exploding wire technique based on resistive heating is suitable to get information on the vapor pressure of metals as a function of enthalpy at extreme temperatures. Measurements are generally confined to such materials which allow to maintain a uniform sample resistivity in the liquid phase region.

Both electron beam heating and neutron pulse heating allow direct measurement of saturation vapor pressures versus enthalpy. These techniques represent promising methods to determine the vapor pressure of ceramic fuel samples up to the vicinity of the critical region. From the uncertainties of the energy deposit within the sample bounds on uncertainty can be defined for the resulting vapor pressure curve.

Laser pulse heating techniques allow vapor pressure measurements as a function of temperature with ceramic fuel materials between some 3500 K and 5000 K. In general, the saturation vapor pressure curve cannot be measured directly corresponding to open surface evaporation and the condition of forced congruent evaporation. But measured vapor pressures can be converted to closed system conditions to establish the required EOS. An upper temperature limit of vapor pressure measurement and pyrometric temperature measurement is given by the increasing radiational interaction

of the laser light and of the thermal temperature radiation with the ionized vapor plume.

4. A METHOD OF VAPOR PRESSURE MEASUREMENT USING LASER BEAM HEATING

In the following, a short description is given of the KfK vapor pressure measurements with UO_2 using a laser beam heating technique /24, 26/.

The measuring principle is shown in Fig.4.1. An electromagnetic chopper-shutter system cuts out a 1 to 10 msec long pulse of exactly constant power from the continuous laser beam of a 500-Watt CO_2 laser. With a special rotating wobble mirror, the laser beam is directed into the vacuum chamber and is focused at the specimen being fixed on the target revolver. The rotating mirror causes the laser focus to move uniformly on a circular trace over the specimen surface. This procedure ensures a defined and reproducible local heating of the specimen surface and allows the evaporation of a relatively large sample from a flat crater. The vapor is collected with a ballistic pendulum collector suspended from a microbalance. In this way, mass and momentum of the off-flowing vapor can be measured precisely.

The radial temperature distribution of the evaporation area, T(r), and the course of the surface temperature with time during the laser pulse, T(r,t), are measured with a fast micropyrometer. This special monochromatic pyrometer with sighting telescope allows temperature measurements of microscopic surface areas (35 µmϕ) with fast time resolution (~1µs) at low noise level. The evaluation of

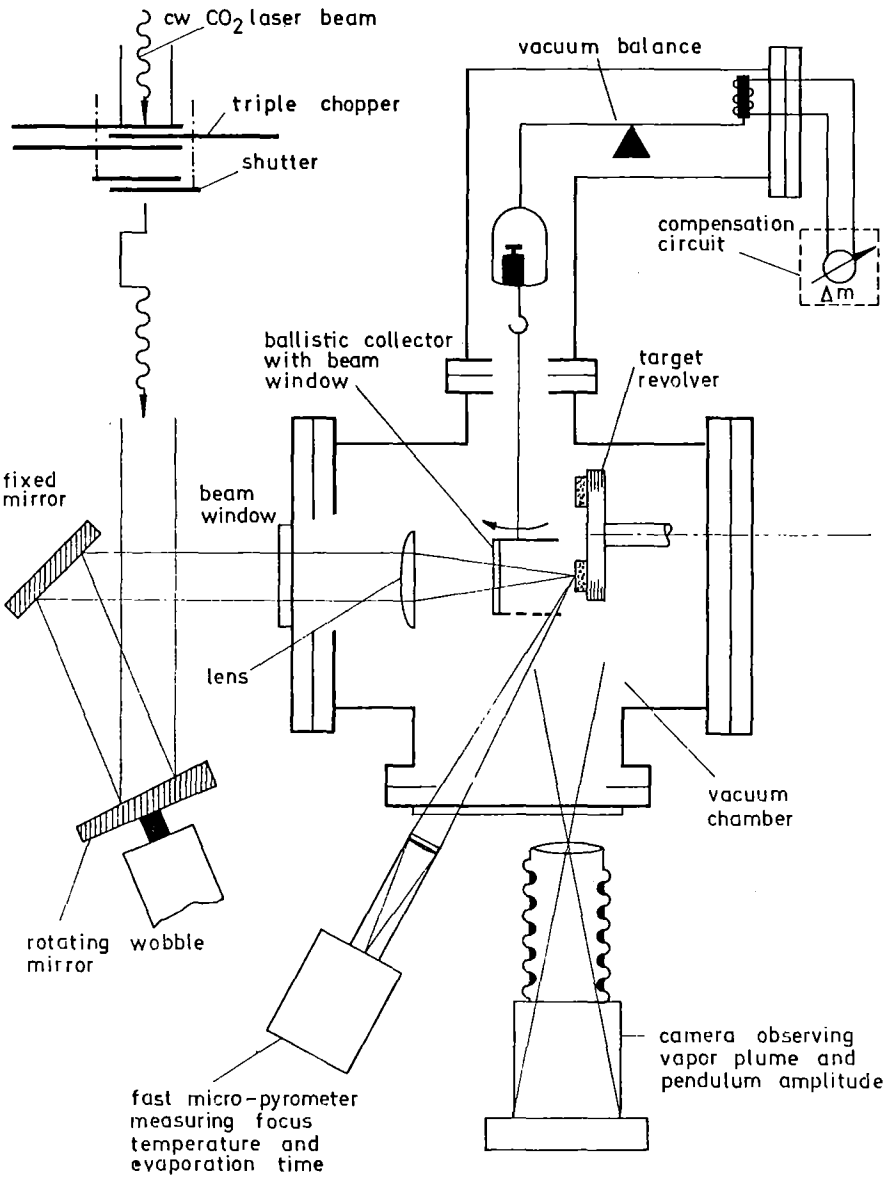

Fig.4.1 Principle of the vapor pressure measuring technique.

the true surface temperature from the pyrometrically measured black-body temperature requires the knowledge of the spectral emissivity of the specimen surface at the actual temperature. For this reason, the spectral emissivity of nuclear fuel materials (UO_2, UC) at the pyrometer wavelength (0.63 µm) has been measured up to temperatures extending far into the liquid range (~4000 K). The emissivity measurements are described in the next chapter.

For the evaluation of the required saturated vapor pressure $p_s(T)$ from open-evaporation experiments, a suitable theoretical evaluation model is needed which describes quantitatively with sufficient accuracy the essential phenomena of intensive surface evaporation into vaccuum by laser heating. The essential points are: quantitative description of the strong concentration gradients arising in the evaporating specimen in intensive surface evaporation /3, 42/, correct treatment of the liquid-vapor phase boundary (problems: thermodynamic or thermal equilibrium, accomodation coefficients of the vapor species, plasma boundary phenomena) /5, 26, 42/, description of the gas dynamic vapor flow-off (problems: gas dynamic expansion of the vapor jet with partial relaxation of the internal degrees of freedom, thermodynamic state and kinetic behavior of the expanding vapor, plasma and cluster phenomena) /5, 24, 26, 41/.

The theoretical evaluation procedure used in the vapor pressure measurements with liquid urania is characterized as follows:

Concerning the difference between the saturated vapor pressure measured in open, forced-congruent evaporation of the UO_{2-x} specimen and the required saturation pressure of the bulk material, it has been shown theoretically that the deviation between the two saturation vapor pressures

is insignificant in the case of UO_2 up to temperatures of about 4500 K /3, 45/. In these thermodynamic calculations, thermodynamic equilibrium has been assumed to exist at the vapor-liquid phase boundary /42/.

The gas dynamic model used to describe the vapor flow-off into vacuum /26, 41/ is summarized in the set of equations (4.1) to (4.6). In these equations the measuring quantities, reaction force $\dot{I}$, mass rate of evaporation $\dot{m}$, evaporation temperature T, are linked to the required saturated vapor pressure $p_s(T)$. The physical conception of this model is as follows: The vapor effusing from the evaporating surface expands adiabatically immediately above the laser focus area to the local velocity of sound and passes over to a supersonic flow with the final velocity w. By use of Laval's theory for a Mach-1 nozzle together

$$\dot{I} = \dot{m} \cdot w_{eff}, \quad w = K_\Theta \cdot w_{eff}; \quad (UO_2: K_\Theta \approx 1.4) \tag{4.1}$$

$$\Delta H = \frac{M}{2} \cdot w^2 = (f_{relax} + 2) \cdot \frac{RT}{2}, \tag{4.2}$$

$$\frac{\dot{m}}{F} = \rho \cdot g_1(f_{relax}) \cdot \sqrt{\frac{RT}{M}}; \quad (UO_2: f_{relax} \approx 5) \tag{4.3}$$

M: molecular weight; F: evaporation area

$$p_o = \frac{\rho}{M} \cdot RT,$$

$$p_{react} = \frac{\dot{m}}{F} \cdot w_{eff} = p_o \cdot g_2(f_{relax})/K_\Theta, \tag{4.4}$$

$$p_s = \frac{2}{1+b} \cdot p_o \qquad 0<b<1, \tag{4.5}$$

$$a) \quad p_s = const \cdot p_{react}; \qquad b) \quad p_s = konst \cdot \frac{\dot{m}}{F} \cdot \sqrt{\frac{RT}{M}} \tag{4.6}$$

with the adiabatic equation of state, the relation (4.3) is obtained between the measured mass of evaporation $\dot{m}/F$ and the density ρ and the temperature T of the vapor at the evaporating surface. The numerical expression $g(f_{relax})$ depends only on the number of the actually relaxating degrees

of freedom of the vapor expansion. With the ideal gas law, from Eqs.(4.2) and (4.3) Eq.(4.4) is obtained which represents a relation between the reaction pressure, p_{react}, and the static vapor pressure, p_o, of the vapor before its expansion into the vacuum. The vapor layer at the evaporating surface, however, cannot be assumed to be saturated. Nor the contrary can be assumed to occur in intensive surface evaporation: free molecular evaporation. The reality lies between these two limiting cases. This is taken into account in Eq.(4.5) by the back-scattering factor b which is set to the medium value of 0.4. The accomodation coefficients of the vapor species being back-scattered to the evaporating surface have been set to 1.

Summarizing the equations (4.3) to (4.5), two independent expressions are obtained for the required saturated vapor pressure $p_s(T)$: By Eq. (4.6a) p_s is related to the reaction pressure, while by Eq.(4.6b) p_s is related to the mass rate of evaporation and to the evaporation temperature.

The radial distribution of temperature of the laser focus area is not isothermal. However, by integration over the temperature distribution actually measured of the evaporation area, the isothermally related quantities - reaction pressure, mass rate density of evaporation, and temperature - can be directly determined. The evaluation procedure is based on the set of equations (4.7) to (4.12).

The measuring quantities used are: the momentum I and evaporated mass Δm, the evaporation time τ, the central temperature T_o in the focus area, and the temperature distribution of the focus area, $T(r,\phi)$. Eq.(4.7a) represents the total reaction force of the vapor jet on the specimen which is equal to the area integral of the reac-

tion pressure $p_{react.}$. Eq.(4.8a) is the corresponding relation for the local reaction force acting in the focus center area Δf_o. Dividing the two equations leads to a recursion formula (4.9a) from which the local reaction pressure in the focus center, $p_{react.}(T_o)$, is obtained. By substituting the reaction pressure by Eq.(4.10a) (cf.Eq.(4.6)) one gets from Eq.(4.11) the required saturated vapor pressure p_s at the central temperature T_o. The recursion can be started with a rough approximation of the saturated vapor pressure curve, $p_s^o(T)$. The initial iterate can be taken, e.g., from a first evaluation of the experimental measuring data using Eq.'s (4.1) to (4.6), or an extrapolated vapor pressure curve is used for $p_s^o(T)$. The successive approximation for $p_s(T_o)$ then quickly converges.

$$I, \Delta m, \tau, T_0, T(r,\varphi)$$

(4.7a) $$\dot{I}_{total} = \frac{I}{\tau} = \iint p_{react.}(T(r,\varphi)) \cdot df$$

(4.7b) $$\dot{m}_{total} = \frac{\Delta m}{\tau} = \iint v_{evap.}(T(r,\varphi)) \cdot df$$

(4.8a) $$\dot{I}_0 = p_{react.}(T_0) \cdot \Delta f_0$$

(4.8b) $$\dot{m}_0 = v_{evap.}(T_0) \cdot \Delta f_0$$

(4.8a):(4.7a)

(4.9a) $$p_{react.}^{i+1}(T_0) = \frac{p_{react.}^{i}(T_0)}{\iint p_{react.}^{i}(T(r,\varphi)) \cdot df} \cdot \frac{I}{\tau}$$

(4.8b):(4.7b)

(4.9b) $$v_{evap.}^{i+1}(T_0) = \frac{v_{evap.}^{i}(T_0)}{\iint v_{evap.}^{i}(T(r,\varphi)) \cdot df} \cdot \frac{\Delta m}{\tau}$$

(4.10a) $$p_s(T) = \text{const} \cdot p_{react.}(T)$$

(4.10b) $$p_s(T) = \text{konst} \cdot v_{evap.}(T) \cdot \sqrt{RT/M}$$

$$p_s^i(T) = \alpha^i \cdot \exp(-Q^i/T) \quad ; Q^i = Q^i(T)$$

(4.11) $$p_s^{i+1}(T_0) = \text{const} \cdot \frac{p_s^i(T_0)}{\iint p_s^i(T(r,\varphi)) \cdot df} \cdot \frac{I}{\tau}$$

(4.12) $$p_s^{i+1}(T_0) = \text{konst} \cdot \sqrt{\frac{R}{M}} \cdot \frac{p_s^i(T_0)}{\iint p_s^i(T(r,\varphi))/\sqrt{T(r,\varphi)} \cdot df} \cdot \frac{\Delta m}{\tau}$$

In addition, the saturation vapor pressure $p_s(T_o)$ can be determined, independently from the method above from the measured mass rate of evaporation, $\Delta m/T$. An analogous deduction leads from Eq.'s (4.7b) to (4.10b) to the recursion relation (4.12).

Fig.2.4 shows the results of these vapor pressure measurements with stoichiometric UO_2. As can be seen, p-T data (represented by the circles) lie well within the 70% confidence interval of the theoretically determined vapor pressure curve. Thus, the requirement of fast reactor safety analysis seems to be fulfilled, i.e., the total limit of error of the fuel vapor pressure curve should not exceed a factor of 2.

Concerning the vapor pressure measurements, however, one should not overvalue this good coincidence between the experimental p-T data measured up to now, and the theoretically deduced vapor pressure curve of liquid UO_2. As has been indicated above, there still are open questions in the physical description of the phenomena occuring in intensive surface evaporation generated by laser heating. Not proven assumptions have been made for the present to overcome these problems in the evaluation of the evaporation experiments.

If, for instance, the accomodation coefficients α of the vapor molecules would turn out to be smaller than 1, this would mean a shift of the measured p-T data to higher pressure values. In the case of a free molecular evaporation model, the resulting vapor pressure curve would have been shifted by a factor of $1/\alpha$. In the case of the gas dynamic evaluation used in the measurements described above, the p-T data would be shifted by $(1-0.4(1-\alpha))/\alpha$.

5. MEASUREMENT OF THERMAL RADIATION PROPERTIES OF UO_2

The knowledge of the spectral emissivity at a few defined wavelengths and its dependence on temperature and stoichiometry, $\varepsilon_\lambda(T,...)$, allows reliable pyrometric temperature measurements of a liquid fuel surface up to about 4000 K. This serves to improve the reliability of the vapor pressure curves of liquid fuel materials when these are measured in open evaporation experiments, e.g., by using a laser heating technique. Beyond, the spectral course and angular distribution of the thermal emittance and reflectance, and its dependence on the polarization yield informations on the physical structure and the bonding character of the material investigated. Up to now experimental results to these questions were lacking at all for the liquid phase of nuclear fuel materials. - The measurement of $\varepsilon_\lambda(T)$ at wavelengths extending to the UV and IR also allows to evaluate the total hemispherical emissivity, $\varepsilon_\Delta(T)$. The knowledge of the total emittance is relevant to problems in reactor safety analysis in which the thermal radiation of molten core material is involved.

For measuring the spectral reflectance and emittance of ceramic fuel materials at temperatures extending far into the liquid range, an integrating sphere laser reflectometer has been developed - using laser beam heating and monochromatic irradiation of the specimen with modulated polarized laser light. The spectral range covered extends from the near UV through the visible and near IR (using Kr-ion and HeNe laser lines) to the far IR (using the CO_2 laser line). The surface temperature of the laser-heated specimen is measured with a fast monochromatic pyrometer /43/.

Fig.51 shows the principle of the measuring method and of the experimental set-up. The small fuel specimen is located in the integrating sphere of uniform high diffuse

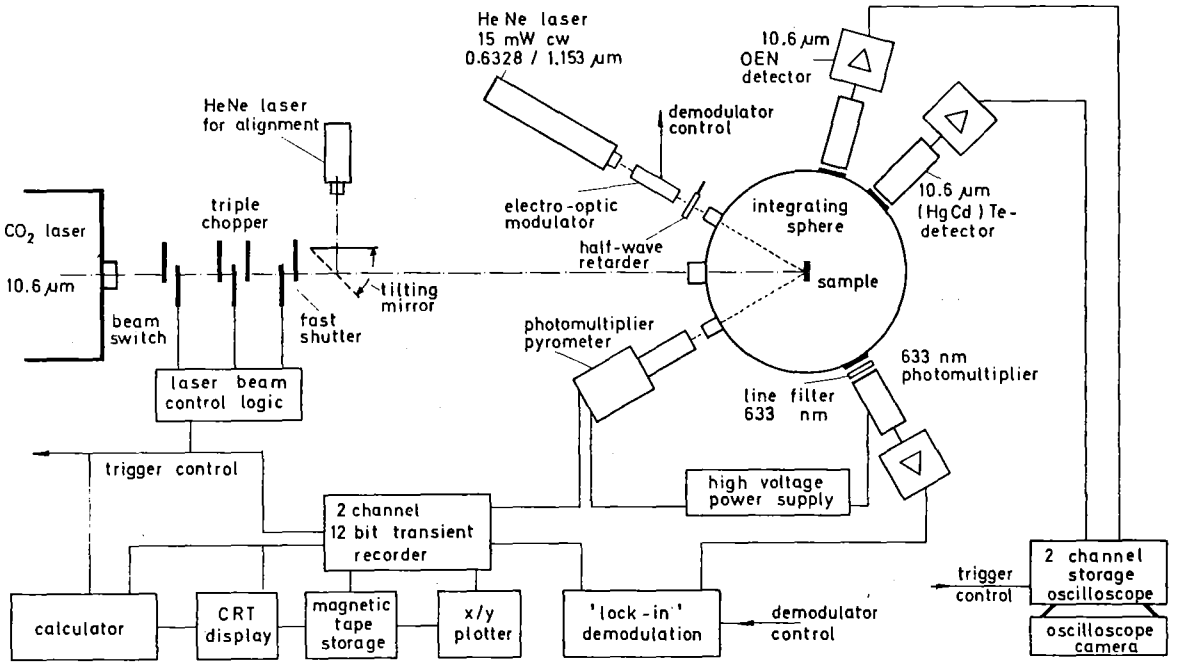

Fig.5.1 Principle of the measuring method and of the experimental set up.

reflectance having 200 mm in diameter. Two spheres are used with different surface coatings for measurements in the near UV, in the visible and near infrared spectral range, and in the far infrared range, respectively. An inert gas pressure level can be adjusted in the spheres from vacuum to ~2 bar.

A 1 to 10 ms long rectangular CO_2 laser pulse of 500 Watt constant power level is focused on the specimen surface which becomes locally heated to the liquid state. The temperature and the heating rate at the molten specimen surface are varied by variation of the focused laser power density. Simultaneously with the heating high-power laser beam, the focus center at the specimen surface is irradiated with the sharply focused reference light beam at the wavelength λ. To overcome measuring problems arising from the intense thermal radiation emitted from

the heated specimen area, a modulated polarized laser beam has to be used as the reference light source. A Krypton ion laser and a HeNe laser are used to cover the spectral region from the near UV to the near IR.

The reflected portion of the incident reference light is isotropically scattered in the integrating sphere and is measured with a fast photomultiplier detector. A spectral line filter of wavelength λ is located in front of the detector to block the thermal radiation emitted by the sample. In order ro suppress any residual thermal radiation let through the blocking filter and to enhance the signal to noise ratio, the detected signal of the modulated reference light is demodulated by a phase-sensitive lock-in technique.

For the evaluation of the directional-hemispherical reflectivity of the sample, $\rho_\lambda(\theta;2\pi)$, a similar measurement is made on a comparison standard using a fully-reflecting mirror instead of the heated sample. The angle θ of incidence or emission, respectively, is varied by altering the incline of the sample. The angle of polarization can be varied with the half-wave retarder. The course of the sample temperature, T(t), is measured with the fast micropyrometer described in Ch.4.

The reflectivity $\rho_\lambda(\theta;\ 2\pi)$ of an opaque material is related to the required directional emissivity $\varepsilon_\lambda(\theta)$ by Kirchhoff's law

$$\varepsilon_\lambda(\theta) = 1 - \rho_\lambda(\theta;\ 2\pi). \qquad (5.1)$$

In the visible range at 0.633 µm wavelength measurements have been performed with sintered and premolten UO_2 specimens at temperatures up to 4000 K and at angles of incidence θ from 7.5 to 45° /43/. The results are shown in Fig.5.2. The width of the shadowed data fields represents the ranges of uncertainty.

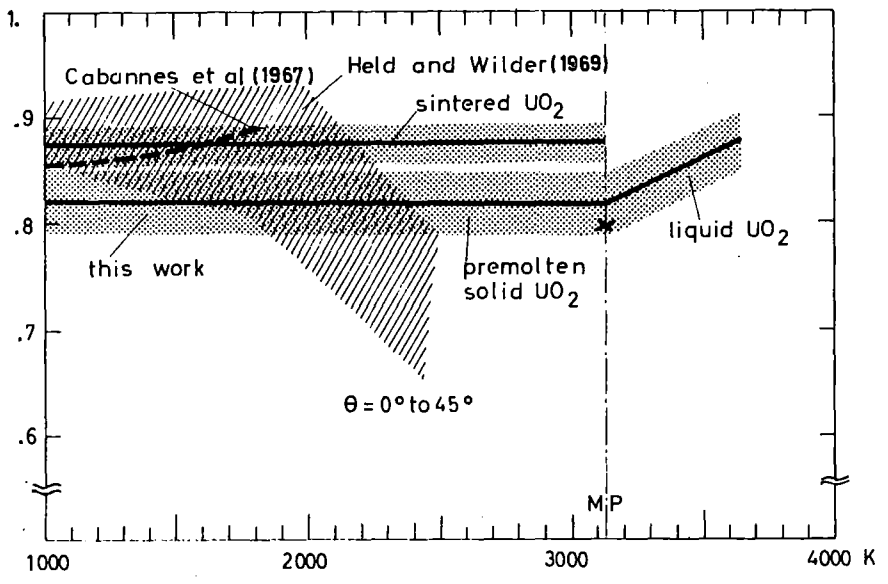

Fig.5.2 Directional emissivity $\varepsilon_{0.633}$ of solid and liquid UO_2 at 0.633 µm as a function of temperature /43/. For comparison the measurements of Cabannes and Held and Wilder are also shown.

At the melting point of UO_2 the difference in the emissivity of sintered and premolten samples vanishes; the measurements yield an emissivity value of

$$\varepsilon_{0.633}(Tm) = 0.81 \pm 0.03.$$

Above the melting point the emissivity of UO_2 increases with temperature and reaches a value of 0.87 ± 0.03 at 3700 K.

Thermodynamic Functions (kJ/mol)
for urania and urania-plutonia solutions

	$\Delta G_{f,T}(UO_2(\ell))$ Ref./4,13/	$\Delta G_{f,T}(UO_3(g))$ /11/	$\Delta G_{f,T}(UO_2(g))$ /4,13/	$\Delta G_{f,T}(UO(g))$ /2/	$\Delta G_{f,T}(U(g))$ /2/	$\Delta G_{f,T}(O(g))$ /22/	$\Delta \bar{G}_{O_2}(UO_2)$ /16,17/
3120K ($T_m(UO_2)$)	-552.0	-581.9	-462.6	-212.8	+139.0	+46.49	-257.5
3200K	-541.6	-574.4	-462.2	-217.4	+130.0	+41.08	-241.1
3400K	-516.4	-555.7	-460.9	-229.0	+107.4	+27.56	-201.0
3600K	-491.8	-537.0	-459.4	-240.5	+ 84.80	+14.04	-162.1
3800K	-467.6	-518.3	-457.8	-252.1	+ 62.20	+ 0.52	-124.4
4000K	-444.0	-500.0	-456.0	-263.6	+ 39.60	-13.00	- 87.62
4200K	-420.6	-480.9	-454.1	-275.2	+ 17.00	-26.52	- 51.77
4400K	-397.6	-462.1	-452.1	-286.7	- 5.60	-40.04	- 16.72
4600K	-375.0	-443.4	-450.0	-298.2	- 28.20	-53.56	+ 17.58
4800K	-352.7	-424.7	-447.7	-309.8	- 50.80	-67.08	+ 51.21
5000K	-330.8	-406.0	-445.3	-321.3	- 73.40	-80.60	+ 84.21

((U,Pu)mixed oxide: $U_{1-x}Pu_xO_{2-y}$, $V_{Pu}=4-2y/x=4-2z=20/Pu$)

	$\Delta G_{f,T}(PuO_{2-z}(\ell))$ /2,3,6/			$\Delta G_{f,T}(PuO_2(g))$	$\Delta G_{f,T}(PuO(g))$	$\Delta G_{f,T}(Pu(g))$	$\Delta \bar{G}_{O_2}(U_{0.8}Pu_{0.2}O_{2-y})$ /16,17/		
	($V_{Pu}=4$)	($V_{Pu}=3.7$)	($V_{Pu}=3.5$)	/2, 3, 6/	/2, 3, 6/	/2, 3, 6/	($V_{Pu}=4$)	($V_{Pu}=3.7$)	($V_{Pu}=3.5$)
	PuO_2	$PuO_{1.85}$	$PuO_{1.75}$				O/M=2	O/M=1.97	O/M=1.95
3120K ($Tm(UO_2)$)	-487.4	-4 95.5	-481.4	-384.3	-245.8	+ 53.45	-135.0	-186.7	-220.7
3200K	-475.1	-485.3	-471.9	-382.1	-249.1	+ 46.42	-123.6	-172.1	-204.1
3400K	-445.1	-460.5	-448.7	-376.5	-257.2	+ 28.84	- 95.03	-136.3	-163.9
3600K	-415.7	-436.3	-426.2	-371.0	-265.3	+ 11.27	- 66.60	-101.6	-125.2
3800K	-387.1	-412.9	-404.4	-365.4	-273.4	- 6.31	- 38.27	- 67.81	- 87.91
4000K	-359.0	-390.0	-383.2	-359.8	-281.6	- 23.88	- 10.02	- 34.85	- 51.87
4200K	-331.5	-367.7	-362.5	-354.3	-289.7	- 41.45	+ 18.15	- 2.65	- 16.94
4400K	-304.4	-345.8	-342.3	-348.7	-297.8	- 59.03	+ 46.26	+ 28.88	+ 16.96
4600K	-277.8	-324.4	-322.6	-343.1	-305.9	- 76.60	+ 74.30	+ 59.78	+ 49.93
4800K	-251.6	-303.4	-303.3	-337.6	-314.0	- 94.18	+102.3	+ 90.12	+ 82.05
5000K	-225.8	-282.8	-284.3	-332.0	-322.2	-111.8	+130.2	+119.9	+113.4

Equations for the Thermodynamic Functions for Urania and Urania-Plutonia Solutions (kJ/mol) (T_m<T<5000 K)

$$\Delta G_{f,T}(UO_2(\ell)) = -2088+0.0773\cdot T + 370.6\cdot \log T$$

$$\Delta G_{f,T}(UO_3(g)) = -873.8+0.09356\cdot T$$

$$\Delta G_{f,T}(UO_2(g)) = -124.9 + 0.02186\cdot T - 116.2\cdot \log T$$

$$\Delta G_{f,T}(UO(g)) = -32.64 - 0.05774\cdot T$$

$$\Delta G_{f,T}(U(g)) = 491.6 - 0.113\cdot T$$

$$\Delta G_{f,T}(O(g)) = 257.4 - 0.0676\cdot T$$

$$\Delta \bar{G}_{O_2}(UO_2) = -3423 + 0.092\cdot T + 823.8\cdot \log T$$

$$\Delta G_{f,T}(PuO_{2.00}(\ell)) = -2486 + 0.0851\cdot T + 496\cdot \log T, \qquad (V_{Pu}=4)$$

$$\Delta G_{f,T}(PuO_{1.85}(\ell)) = -2413 + 0.0591\cdot T + 496\cdot \log T, \qquad (V_{Pu}=3,7)$$

$$\Delta G_{f,T}(PuO_{1.75}(\ell)) = -2373 + 0.0508\cdot T + 496\cdot \log T, \qquad (V_{Pu}=3.5)$$

$$\Delta G_{f,T}(PuO_2(g)) = -471.1 + 0.02782\cdot T$$

$$\Delta G_{f,T}(PuO(g)) = -119.2 - 0.04059\cdot T$$

$$\Delta G_{f,T}(Pu(g)) = 327.6 - 0.08787\cdot T$$

$$\Delta \bar{G}_{O_2}(U_{0.8}Pu_{0.2}O_{2.00}) = -794.4+0.1335T+69.51\cdot \log T, \qquad (V_{Pu}=4)$$

$$\Delta \bar{G}_{O_2}(U_{0.8}Pu_{0.2}O_{1.97}) = -2879+0.0877T+692.2\cdot \log T, \qquad (V_{Pu}=3.7)$$

$$\Delta \bar{G}_{O_2}(U_{0.8}Pu_{0.2}O_{1.95}) = -4043+0.06485T+1036\cdot \log T, \qquad (V_{Pu}=3.5)$$

PARTIAL VAPOR PRESSURES (BAR)

$UO_{2.00}$ ($T_{melt.}$=3120 K; $T_{boil.}$ = 3700 K)

	P_{UO_3}	P_{UO_2}	P_{UO}	P_U	P_{O_2}	P_O	P_{total}	O/U-vapor
3120 K	0.022	0.032	3E-4	6E-8	3E-7	1E-4	0.055	2.40
3500 K	0.190	0.222	0.002	6E-7	6E-5	0.004	0.417	2.46
4000 K	1.43	1.44	0.017	7E-6	0.002	0.070	2.95	2.52
4500 K	5.96	5.65	0.081	5E-5	0.230	1.68	13.6	2.69
5000 K	16.9	15.8	0.290	3E-4	2.58	11.2	46.8	3.00

$(U_{0.8}Pu_{0.2})O_{2.00}$

	P_{UO_3}	P_{UO_2}	P_{UO}	P_U	P_{PuO_2}	P_{PuO}	P_{Pu}	P_{O_2}	P_O	P_{total}
3120K	0.188	0.026	2E-5	4E-10	0.004	2E-4	3E-8	0.002	0.008	0.229
3500K	0.855	0.178	3E-4	1E-8	0.029	0.002	6E-7	0.028	0.081	1.18
4000K	3.67	1.15	0.004	5E-7	0.205	0.023	1E-5	0.368	0.900	6.32
4500K	10.6	4.52	0.029	8E-6	0.867	0.119	1E-4	2.69	5.73	24.6
5000K	23.5	12.7	0.134	7E-5	2.57	0.424	0.001	13.0	25.0	77.3

$(U_{0.8}Pu_{0.2})O_{1.97}$

	P_{UO_3}	P_{UO_2}	P_{UO}	P_U	P_{PuO_2}	P_{PuO}	P_{Pu}	P_{O_2}	P_O	P_{total}
3120K	0.070	0.026	6E-5	3E-9	0.002	3E-4	1E-7	7E-5	0.001	0.098
3500K	0.444	0.178	0.001	5E-8	0.011	0.002	9E-7	0.003	0.029	0.668
4000K	2.53	1.15	0.006	1E-6	0.075	0.012	9E-6	0.121	0.514	4.41
4500K	8.57	4.52	0.036	1E-5	0.292	0.050	5E-5	1.47	4.24	19.2
5000K	20.7	12.7	0.151	9E-5	0.811	0.151	2E-4	9.23	21.1	64.9

$(U_{0.8}Pu_{0.2})O_{1.95}$

	P_{UO_3}	P_{UO_2}	P_{UO}	P_U	P_{PuO_2}	P_{PuO}	P_{Pu}	P_{O_2}	P_O	P_{total}
3120K	0.036	0.026	1E-4	1E-8	0.002	0.001	4E-7	6E-6	4E-4	0.065
3500K	0.287	0.178	0.001	1E-7	0.012	0.003	2E-6	7E-4	0.013	0.494
4000 K	1.96	1.15	0.008	2E-6	0.082	0.017	2E-5	0.053	0.340	3.60
4500K	7.41	4.52	0.042	2E-5	0.321	0.063	8E-5	0.955	3.41	16.8
5000K	19.1	12.7	0.163	1E-4	0.886	0.179	3E-4	7.39	18.9	59.3

References

1. J.H.Tait, E.A.Khodarev, O.Wilmore (Editors), Proc. IAEA Specialists Meeting on Role of Fission Products in Whole Core Accidents, A.E.R.E. Harwell, UK 1977, IAEA Vienna, p.14-30.

2. R.J.Ackermann, M.S.Chandrasekharaiah, Systematic Thermodynamic Properties of Actinide Metal-Oxygen Systems at High Temperatures, Proc. IAEA Symp. on Thermodynamics of Nuclear Materials 1974, Vol.2, p.3, Vienna 1975.

3. W.Breitung, Berechnung der Dampfdrücke von oxidischen Brennstoffen bis 5000 K bei Gleichgewichts- und Nichtgleichgewichtsverdampfung, Report KFK-2091 (1975).

4. M.H.Rand, R.J.Ackermann, F.Gronvold, F.L.Oetting, A.Pattoret, The Thermodynamic Properties of the Urania Phase, Int.Colloquium on Refractory Oxides for High Temperature Energy Sources, Odeillo, France, June 28-July 1, 1977 , paper B4.

5. H.U. Karow, Thermodynamic State and Gas Kinetic Relaxation Behavior of Saturated UO_2 Vapor up to 5000 K, Report KfK-2390 (1977), and Int. Colloq. on Refractory Oxides for High Temperature Energy Sources, Odeillo, France June 28 - July 1, 1977, paper B3.

6. M.H.Rand, T.L.Markin, Some Aspects of $(U,Pu)O_2$ Solid Solutions and their Use as Nuclear Fuels, Proc. IAEA Symp. on Thermodynamics of Nuclear Materials 1966, p. 637, Vienna 1967.

7. Graf, Henning, Stange,
"Formeln und Tabellen der mathematischen Statistik", p.223 ff., Springer-Verlag, Berlin 1966.

8. R.J.Ackermann, R.J.Thorn,
The Evaporation Behaviour, Thermodynamic Properties and Systematic Trends of Actinide Metal-Oxygen Systems. Proc. IAEA Symp. on Thermodynamics, Vol.1, p.243, Vienna 1966.

9. D.R.Stull, G.C.Sinke,
"Thermodynamic Properties of the Elements",
Amer.Chem.Soc., Washington D.C., 1956.

10. M.Tetenbaum, P.D.Hunt,
High-Temperature Thermodynamic Properties of Oxygen-Deficient Urania. J.Chem.Phys.49,
4739 (1968).

11. S.D.Gabelnick,
Equation of State of UO_2, in LMFBR Safety Annual Report, p.60, ANL-8120 (1974).

12. H.L.Schick,
"Thermodynamics of Certain Refractory Compounds",
Vol.2, 2-255, Academic Press, New York, 1966.

13. M.H.Rand,
private communication (1978).

14. R.J.Ackermann, P.W.Gilles, R.J.Thorn,
High-Temperature Thermodynamic Properties of Uranium Dioxide. J.Chem.Phys. 25, 1089 (1956).

15. A.Pattoret, J.Drowart, S.Smoes,
Etudes Thermodynamiques par Spectrometrie de Masse sur le Systeme Uranium-Oxygene, Proc. IAEA Symp. on Thermodynamics of Nuclear Materials, 1967, p.613, Vienna 1968.

16. P.E.Blackburn,
Chemical Modeling of Mixed-oxide Reactor Fuel Systems, p.5.8 in Report ANL-RDP-35 (1974).

17. M.deFranco, J.P.Gatesoupe,
The Thermodynamic Properties of $(U,Pu)O_{2\pm x}$ Described by a Cluster Model, Proc.Conf. on Plutonium and Other Actinides, p.133, H.Blank and R.Lindner, Eds., North-Holland Publishing Company, Amsterdam 1976.

18. J.Drowart, A.Pattoret, S.Smoes,
Mass Spectrometric Studies of the Vaporization of Refractory Compounds, Proc.Brit.Ceram.Soc.8, 67 (1967).

19. R.J.Ackermann, R.J.Thorn, M.Tetenbaum, C.Alexander,
Free Energies of Formation of Gaseous Uranium, Molybdenum, and Tungsten Trioxides. J.Phys.Chem.64, 350 (1960).

20. C.A.Alexander,
"Vapor-Solid Equilibrium in the Uranium Oxide-Oxygen System", Doctoral Dissertation, Ohio State University, Columbus, Ohio, 1961.

21. R.J.Ackermann, A.T.Chang,
Thermodynamic Characterization of the U_3O_{8-z} Phase, J.Chem.Thermodynamics 5, 873 (1973).

22. D.R.Stull, H.Prophet,
"JANAF Thermochemical Tables", 2nd.Edition, NSRDS 37, Nat.Bur.Stand.(U.S.), 1971.

23. W.L.Lyon,
The Solid-Liquid Phase Diagram for the UO_2-PuO_2 System, J.Nucl.Mater. 22, 332 (1967).

24. M.Bober, W.Breitung, H.U.Karow, K.Schretzmann, Laser-Experimente zur Bestimmung des Dampfdrucks von oxidischem Kernbrennstoff bis zu sehr hohen Temperaturen (3000...5000 K), 41.Physikertagung der Deutschen Physikalischen Gesellschaft, Karlsruhe 1977, to be published.

25. J.F.Babelot, G.D.Brumme, P.R.Kinsman, R.W.Ohse, Vapour Pressure Measurements over Liquid UO_2 and $(U,Pu)O_2$ by Laser Surface Heating up to 5000 K. Reaktortagung DAtF, Mannheim, p.351 (1977).

26. M.Bober, H.-U.Karow, K.Schretzmann, Evaporation Experiments to Determine the Vapour Pressure of UO_2 Fuel (3000-5000 K), Proc.IAEA Symp. on Thermodynamics of Nuclear Materials 1974, Vol.1, p.295, Vienna 1975.

27. G.T.Reedy, M.G.Chasanov, Total Pressure of Uranium-Bearing Species over Molten Urania. J.Nucl.Mater.42, 341 (1972).

28. R.W.Ohse, P.G.Berrie, G.D.Brumme, P.R.Kinsman, Advances in Vapour Pressure Studies over Liquid Uranium Plutonium Oxides up to 5000 K, in "Plutonium and Other Actinides", Eds. H.Blank and R.Lindner, North-Holland Publishing Company, Amsterdam 1976, p. 191.

29. A.Cezairliyan, M.S.Morse, H.A.Berman, C.W.Beckett, High-Speed (Subsecond) Measurement of Heat Capacity, Electrical Resistivity, and Thermal Radiation Properties of Molybdenum in the Range 1900 to 2800 K, J.Res.Nat.Bur.Stand. 74A, 65 (1970).

30. K.W.Henry,
A Technique for Measuring Equilibrium Thermodynamic States of Liquid Metals at High Temperatures and Pressures, Rev.Sci.Instr. 43, 1777 (1972).

31. J.W.Shaner, G.R.Gathers, C.Minichino,
A New Apparatus for Thermophysical Measurements above 2500 K, High Temperatures-High Pressures 8, 425 (1976).

32. M.M.Martynyuk, O.G.Panteleichuk,
The Critical Temperature of Metals by the Method of the Electric Explosion of Wires under Pressure, Teplofizika Vysokikh Temperatur, 14, 1201 (1976); High Temperature 14, 1075 (1976).

33. U.Seydel, W.Fucke,
Sub-Microsecond Pulse Heating Measurements of High Temperature Electrical Resistivity of the 3d-Transition Metals Fe, Co and Ni, Z.Naturforsch. 32a, 994 (1977).

34. L.W.Dietrich, J.F.Jackson,
The Role of Fission Product in Whole Core Accidents, Contribution to Ref.1.

35. D.A.Benson,
Vapor Properties of Gold at Extreme Temperatures by Pulsed-Electron-Beam Measurement, J.Appl.Phys. 47, 4873 (1976).

36. D.A.Benson,
Application of Pulsed Electron Beam Vaporization to Studies of UO_2, Report SAND-77-0429 (1977).

37. D.A.Benson,
Rate Effects in the Dynamic Vaporization of Uranium Dioxide, Trans.Am.Nucl.Soc. 27, 574 (1977).

38. E.Gorham-Bergeron,
Theoretical Considerations of Rate Effects in Uranium Dioxide, Trans.Am.Nucl.Soc. 27, 575 (1977).

39. K.O.Reil,
Effective Equation of State Measurements on Uranium Dioxide, PhD Thesis, University of New Mexico, Albuquerque, NM (May 1977); see also, K.O.Reil, A.W.Cronenberg, Trans.Am.Nucl.Soc.27, 576 (1977).

40. R.W.Ohse, P.G.Berrie, H.G.Bogensberger, E.A.Fischer,
Measurement of Vapour Pressure of $(U,Pu)O_2$ and UO_2 to 5000 K for Fast Reactor Safety Analysis and the Contribution of the Radial Cs Distribution to Fuel Pin Failure, Proc. IAEA Symp. on Thermodynamics of Nuclear Materials 1974, Vol.1, p.307, Vienna 1975.

41. M.Bober, W.Breitung, H.U.Karow, K.Schretzmann,
Evaporation Studies of Liquid Oxide Fuel at Very High Temperatures Using Laser Beam Heating (Gordon Research Conf. on High-Temperature Chemistry, Tilton, N.H., 1976) Report KFK-2366 (1976).

42. M.Bober, W.Breitung, H.U.Karow, K.Schretzmann,
On the Interpretation of Vapor Pressure Measurements on Oxide Fuel at Very-High Temperatures for Fast Reactor Safety Analysis, J.Nucl.Mater. 60, 20 (1976).

43. M.Bober, H.U.Karow,
Measurements of Spectral Emissivity of UO_2 Above the Melting Point, Seventh Symposium on Thermophysical Properties, Ed.A.Cezairliyan, National Bureau of Standards, May-10-12, 1977, Gaithersburg, Maryland, USA.

44. M.Bober, H.U.Karow, K.Schretzmann,
Vapor Pressure Measurements of Oxide Fuel Between 3000 and 5000 K Using Laser Heating, Nuclear Technology 26, 237 (1975).

45. W.Breitung,
Verdampfungskinetik von oxidischen Kernbrennstoffen und ihr Einfluß auf die Spaltstoffentmischung in Reaktorbrennstäben und auf den Brennstoffdampfdruck unter Störfallbedingungen, Report KfK-2240 (1976).

46. P.E.Potter, E.A.Khodarev, P.Browning, M.J.Gillan (Editors), Summary and Recommendations,
Proc. IWGFR/IAEA Specialists' Meeting on Equations of State of Materials of Relevance to the Analysis of Hypothetical Fast Breeder Reactor Accidents, A.E.R.E. Harwell, UK June 19-23 1978, IAEA Vienna.